Zitierweise: *Angew. Chem. Int. Ed.* **2024**, *63*, e202319480
doi.org/10.1002/anie.202319480

Perovskites

Data-Driven Controlled Synthesis of Oriented Quasi-Spherical $CsPbBr_3$ Perovskite Materials

Shaohui Liu[+], Zijian Chen[+], Yingming Liu, Lingjun Wu, Boyuan Wang, Zixuan Wang, Bobin Wu, Xinyu Zhang, Jie Zhang, Mengyun Chen, Hao Huang, Junzhi Ye,* Paul K. Chu, Xue-Feng Yu, Lakshminarayana Polavarapu, Robert L. Z. Hoye, Feng Gao, and Haitao Zhao**

Abstract: Controlled synthesis of lead-halide perovskite crystals is challenging yet attractive because of the pivotal role played by the crystal structure and growth conditions in regulating their properties. This study introduces data-driven strategies for the controlled synthesis of oriented quasi-spherical $CsPbBr_3$, alongside an investigation into the synthesis mechanism. High-throughput rapid characterization of absorption spectra and color under ultraviolet illumination was conducted using 23 possible ligands for the synthesis of $CsPbBr_3$ crystals. The links between the absorption spectra slope (difference in the absorbance at 400 nm and 450 nm divided by a wavelength interval of 50 nm) and crystal size were determined through statistical analysis of more than 100 related publications. Big data analysis and machine learning were employed to investigate a total of 688 absorption spectra and 652 color values, revealing correlations between synthesis parameters and properties. Ex situ characterization confirmed successful synthesis of oriented quasi-spherical $CsPbBr_3$ perovskites using polyvinylpyrrolidone and Acacia. Density functional theory calculations highlighted strong adsorption of Acacia on the (110) facet of $CsPbBr_3$. Optical properties of the oriented quasi-spherical perovskites prepared with these data-driven strategies were significantly improved. This study demonstrates that data-driven controlled synthesis facilitates morphology-controlled perovskites with excellent optical properties.

The controlled synthesis of crystals enables the precise manipulation of material properties,[1] crystal structures,[2] and morphologies,[3] thus playing a pivotal role in various applications. For instance, nanowires, nanosheets, and nanocubes have been employed in polarized light emissions,[4] photodetectors,[5] and light-emitting diodes,[6] respectively. However, traditional controlled synthesis methods necessitate the characterization of different samples using techniques such as scanning electron microscopy (SEM), transmission electron microscopy (TEM), and X-ray diffraction (XRD), rendering the process laborious, time-consuming, and costly.

[*] S. Liu,[+] Z. Chen,[+] L. Wu, Z. Wang, B. Wu, X. Zhang, J. Zhang, H. Zhao
Center for Intelligent and Biomimetic Systems, Shenzhen Institute of Advanced Technology, Chinese Academy of Sciences, Shenzhen 518055, Guangdong, PR China
E-mail: ht.zhao@siat.ac.cn

S. Liu,[+] B. Wu, J. Zhang
Nano Science and Technology Institute, University of Science and Technology of China, Suzhou 215000, PR China

S. Liu,[+] Z. Chen,[+] B. Wang, Z. Wang, B. Wu, X. Zhang
Wenzhou Institute of Technology, Digital Intelligent Manufacturing Research Center, Wenzhou 325000, PR China

Z. Chen[+]
Department of Chemical and Environmental Engineering, the University of Nottingham Ningbo China, Ningbo 315100, PR China

Y. Liu
Centre for Photonics Information and Energy Materials, Shenzhen Institute of Advanced Technology, Chinese Academy of Sciences, Shenzhen 518055, Guangdong, PR China

M. Chen, F. Gao
Department of Physics, Chemistry and Biology (IFM), Linköping University, Linköping SE-58183, Sweden

H. Huang, X.-F. Yu
Materials Interfaces Center, Shenzhen Institute of Advanced Technology, Chinese Academy of Sciences, Shenzhen 518055, Guangdong, PR China
E-mail: hao.huang@siat.ac.cn

J. Ye, R. L. Z. Hoye
Inorganic Chemistry Laboratory, University of Oxford, South Parks Road, Oxford OX1 3QR, United Kingdom
E-mail: junzhi.ye@chem.ox.ac.uk

P. K. Chu
Department of Physics, Department of Materials Science and Engineering, and Department of Biomedical Engineering, City University of Hong Kong, Tat Chee Avenue, Kowloon, Hong Kong, China

L. Polavarapu
CINBIO, Materials Chemistry and Physics Group, University of Vigo, Campus Universitario Marcosende, Vigo 36310, Spain

[+] These authors contribute equally to this work.

Recently, data-driven and high-throughput strategies have emerged as promising solutions for crystal-controlled synthesis by collecting large amounts of data,[7] thereby simultaneously characterizing multiple samples, which reduces the need for labor-intensive characterization. Data-driven approaches involve the generation of extensive datasets through the integration of computational and experimental methods, supplemented by sophisticated machine learning (ML) techniques, data has become the new resource, and knowledge is derived from materials datasets.[8] This method of accelerating experiments[8a,9] and characterization facilitates the rapid exploration of the correlation between synthesis parameters and material properties, enabling further investigation into the synthesis mechanism. While high-throughput experimentation is a scientific and experimental approach aimed at improving experimental efficiency by simultaneously processing a large number of samples or data,[10] which commonly serves as the precondition of data-driven.

Materials such as ZnO, Cu_2O, and graphene have recently been prepared via controlled synthesis by changing the temperature,[3] synthesis parameters,[2] and gas environment.[11] Among these materials, perovskites are distinct because of their superior optical properties,[12] long fluorescence lifetimes[13] and tunable band gaps.[14] However, their sensitivity to environmental factors, such as water and oxygen,[15] makes the controlled synthesis of perovskites challenging. Compared with other perovskites, $CsPbBr_3$ is more chemically stable,[16] demonstrating high optical stability.[17]

In this study, the controlled synthesis of oriented quasi-spherical $CsPbBr_3$ perovskites was achieved using data-driven strategies. Considering the instability of small $CsPbBr_3$ crystals in polar solvents,[18] the goal was to create larger, more stable $CsPbBr_3$[19] crystals and identify optimal ligands. Initially, 23 potential ligands were screened,[20] including 15 containing nitrogen, 12 containing hydroxyl groups, and 10 containing carbonyl groups. These functional groups are essential for ligands to interact with the surface of perovskites.[21] Second, literature data revealed a potential correlation between the $CsPbBr_3$ absorption spectra slope (400–450 nm) and the crystal size.[22] Furthermore, ML was employed to determine the optimal synthesis of diverse $CsPbBr_3$ forms and sizes. Moreover, ex situ analyses and density functional theory (DFT) calculations demonstrated how ligands control the size and influence crystallinity. Finally, the photoluminescence quantum yield (PLQY) of quasi-spherical $CsPbBr_3$, synthesized under data-driven guidance, exhibited a ten-fold improvement compared to that of ligand-free samples. Controlled synthesis guided by data-driven strategies can potentially lead to a more efficient design of new and optimized materials with superior properties.

The data-driven controlled synthesis of oriented quasi-spherical $CsPbBr_3$ perovskites relies on high-throughput data collected using a high-throughput rapid characterization platform, which is more than 10 times faster than human analysis. The R, G, and B values (representing the emission intensities of the red, green, and blue primary colors) were captured and extracted using an automated camera to conduct an automated UV/Vis-NIR absorption measurement and using a microplate reader to collect the absorption spectra. Acacia and polyvinylpyrrolidone $(C_6H_9NO)_n$ were identified as the most promising ligands because they produced $CsPbBr_3$ nanocrystals (NCs) with the highest G value and obvious absorption peak(Figure 1a). Single-factor experiments were conducted using polyvinylpyrrolidone (PVP) and Acacia to determine the optimal concentration ranges. In total, 652 G values and 688 absorption spectra were obtained. ML and big data analysis guided the discovery of optimal synthesis conditions, enabling the morphology-controlled synthesis of irregular bulk, cubic bulk, unoriented quasi-spherical structures, and oriented quasi-spherical structures (Figure 1b). In addition, the synthetic mechanism was determined. Finally, oriented quasi-spherical $CsPbBr_3$, screened using data-driven strategies, exhibited significantly improved optical properties (Figure 1c).

High-throughput characterizations of 23 possible ligands were performed to identify their effects on $CsPbBr_3$, including emission color measurements under 365 nm ultraviolet (UV) irradiation and absorption spectra. Ligand selection considered elements and groups that could interact with the perovskites. Hydroxyl groups[23] can influence the growth kinetics and surface state of perovskites, while nitrogen contained functional groups can effectively control the morphology of perovskites and carbonyl groups can coordinate with metal cations, enhancing crystallinity[19] and passivating defect.[24] The G value of the emission color offers a quick assessment of the $CsPbBr_3$ PL intensity because it emits bright green light under 365 nm UV irradiation.

The A1 well (first column in row A on a 24-well plate) served as a ligand-free reference, whereas the other wells tested specific ligands (details are shown in Tables S1–S2). The C3 well (Acacia) exhibited the strongest emission with the highest G value (Figure S1a–b), potentially attributed to Acacia reducing crystal defects or enhancing coupling.[25] After standing overnight exposure to white light, the C4 well (PVP) showed no agglomeration (Figure S2), potentially because PVP improved crystal dispersity. Furthermore, a clear absorption peak can be observed at 526 nm (Figure S3). Inspired by these phenomena, Acacia and PVP were applied together in the synthesis of $CsPbBr_3$, and the optimal synthesis parameters were systematically explored using ML and big data analysis.[26]

To examine the correlation between the absorption spectra and crystal size, more than 100 publications[27] were analyzed (details provided in the Supplementary literature list). A possible correlation between the $CsPbBr_3$ crystal size and the slope was established based on the absorption spectra in the wavelength range of 400–450 nm. A negative slope typically corresponds to nanoscale crystals (Figure 2a and Figure S4). Small crystals (such as quantum dots and NCs) exhibit slopes below 0, whereas larger $CsPbBr_3$ crystals (such as bulk) have slopes equal to or exceeding 0. Notably, the size and slope increased simultaneously in some systems (Figure S5).[28] Meanwhile, in the ligand-assisted reprecipita-

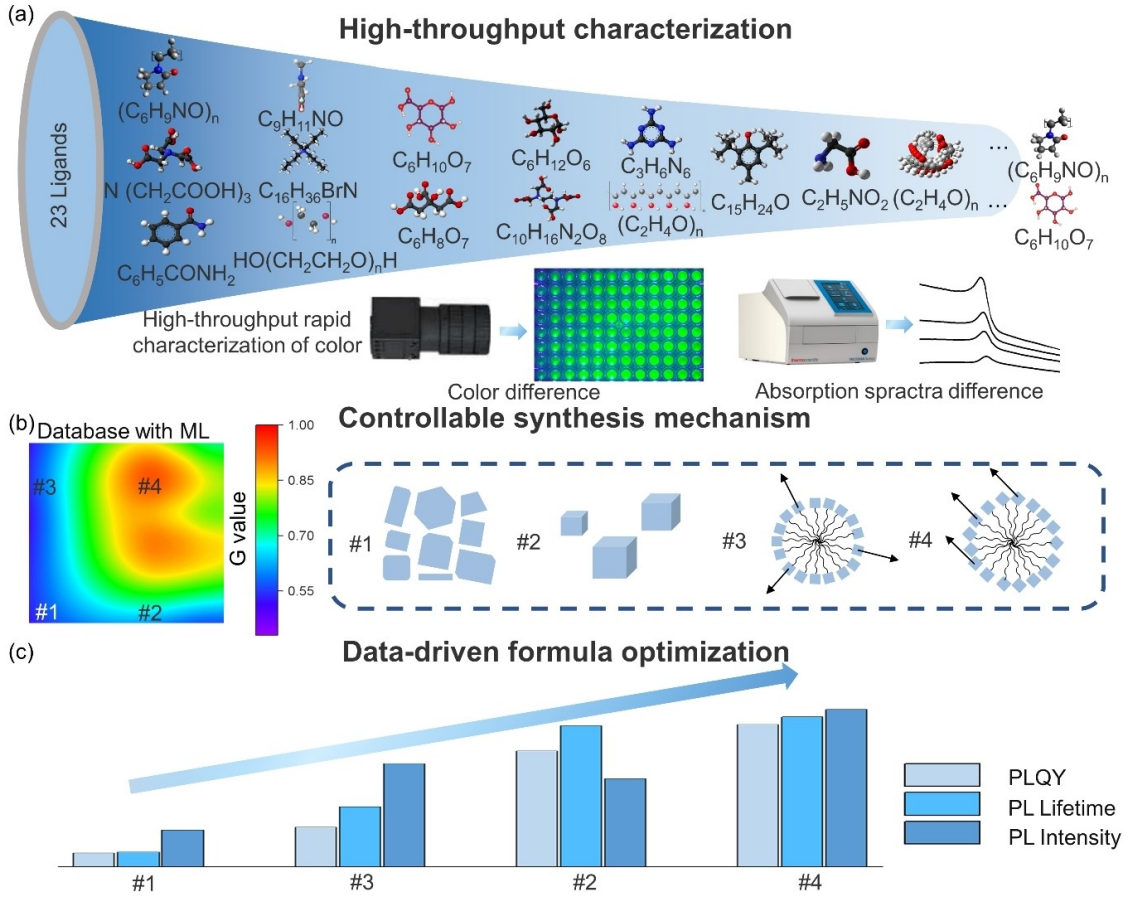

Figure 1. Framework employed for data-driven controlled synthesis of oriented quasi-spherical $CsPbBr_3$ perovskites. (a) Ligand screening through high-throughput rapid characterization of the G value (representing the emission intensities of the green primary color), and using a microplate reader to measure absorption spectra, utilizing a high-throughput characterization platform for simultaneous analysis of up to 96 experimental samples. (b) Establishment of a database by an ML model for morphology-controlled synthesis of CsPbBr3, where the color scale represents the levels of the G value (Symbols: #1 denotes ligand-free, #2 denotes Acacia as ligand, #3 denotes PVP as ligand, and #4 denotes Acacia and PVP as ligands). (c) Data-driven formula optimization for enhanced optical properties.

tion of the crystals, the optimized volume of the anti-solvent ensures the complete precipitation of crystals and influences the size and morphology of these crystals[29] (Figure S6).

Single-factor experiments provided concentration ranges for ligands that enable the synthesis of small-sized particles with high PL intensity. Consequently, based on these results, a double-factor experiment was initiated. Figure 2b shows the variation in the slope for different PVP molecular weights and concentrations. The high-throughput characterization covered 24 PVP concentrations ranging from 0 to 4.8 mM, resulting in 96 absorption spectra (Figure S7). Notably, employing PVP with a molecular weight of 24,000 yielded the smallest slope within the 3.2–4.8 mM range, indicating maximum NC content. The assessment of Acacia encompassed concentrations from 0 to 29 mM, with high-throughput characterizations involving 48 Acacia concentrations, focusing on the PL intensity (Figure S8a–b, Table S3 for G values). The G value increased with increasing Acacia concentration up to 10 mM and then leveled off (Figure S8c).

The double-factor experiment was conducted within the concentration ranges of 3–5.2 mM for PVP (Mw = 24,000) and 4.5–15.5 mM for Acacia based on single-factor experiment outcomes (details are provided in the SI). The sample plate layout and photographs under 365 nm UV irradiation are shown in Figure S9, with the G value analysis summarized in Table S4 and absorption spectra shown in Figure S10. Photographs demonstrate that $CsPbBr_3$ crystals synthesized with PVP and Acacia as ligands exhibited enhanced photoluminescence compared to either PVP or Acacia alone, thereby confirming the synergistic PL enhancement of $CsPbBr_3$ by PVP and Acacia.

Analysis of the absorption spectra of the 556 samples revealed adjustable absorption peaks of $CsPbBr_3$ crystals between 513 and 549 nm owing to the addition of Acacia and PVP (Figure 2c). Statistical analysis of the absorption spectra slope from 400 nm to 450 nm (difference in the absorbance at 400 nm and 450 nm divided by the wavelength interval of 50 nm) was performed to determine the synthesis parameters with maximum NC content. By comparing the slopes of $CsPbBr_3$ synthesized with Acacia only and Acacia

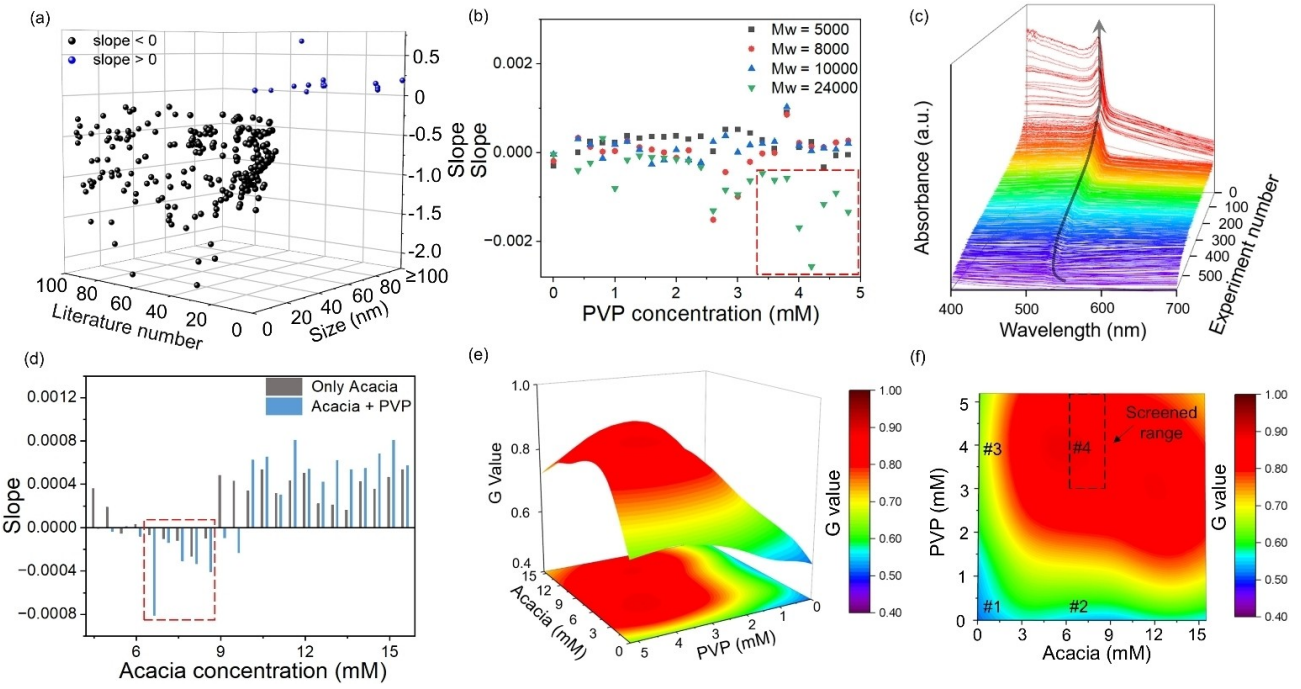

Figure 2. Data-driven optimization of synthesis parameters. (a) Relationship between absorption spectra slope (400–450 nm) and size from related literature data. (b) Absorption spectra slopes based on the single-factor experiment of PVP with four different molecular weights (Mw). (c) Double-factor experiment absorption spectra. (d) Slope in the absorption spectra (400–450 nm) with Acacia only and Acacia with PVP. (Grey bars represent the slopes for each Acacia concentration, and blue bars represent the average of all absorption spectra slopes for the corresponding Acacia concentrations that also contain PVP; the area with the highest NC content is indicated by the red dashed box.) (e) ML model of G value vs. Acacia and PVP concentration (normalized by the highest G value), R^2: 0.71. (f) Bottom projection image of (e), with the black dashed box indicating the screened concentration range. The slopes in (a), (b), and (d) represent the difference in the heights between 450 nm and 400 nm divided by 50. The color scales in (e) and (f) represent the PL intensity of the corresponding synthesis parameter (data normalized to the highest value).

with PVP, the range of Acacia concentrations in which PVP had a significant effect on the particle size was determined (Figure 2d). Before reaching a concentration of 9.5 mM Acacia, the addition of PVP significantly reduced the absorption spectra slope in the 400 nm to 450 nm wavelength range, most notably for Acacia concentrations of 6.5–8.5 mM. Beyond 9.5 mM, this effect was not observed, perhaps indicating a smaller $CsPbBr_3$ crystal size in the range of 6.5–8.5 mM Acacia. In contrast, excessive Acacia led to larger crystal sizes, counteracting the size-reducing effects of PVP.

To determine the concentration range yielding the highest PL intensity, a database of 556 G values was employed for Sure Independence Screening and Sparsifying Operator algorithm training, which is a supervised ML algorithm based on compressed sensing.[30] The 3D surface plot, fitted with predicted data from ML, indicates that Acacia and PVP synergistically enhanced the PL intensity (Figure 2e). Moreover, within the selected Acacia concentration range (6.5–8.5 mM), the PL intensity remains nearly constant irrespective of the PVP concentration within the range of 3–5.2 mM (all fall within the red region) (Figure 2f). Therefore, the selection of the Acacia (6.5–8.5 mM) and PVP concentration range (3–5.2 mM) can be attributed to the potential for a higher abundance of smaller-sized particles and the stronger PL intensity. Thus, the optimal ligands, molecular weights, anti-solvent volumes, and concentrations were determined via high-throughput characterization and data-driven strategies, guiding further exploration into the role of ligands in $CsPbBr_3$ crystals. However, to elucidate the mechanism of ligand interactions, ex situ characterization is required.

Using data-driven strategies and high-throughput experiments, a set of synthesis parameters in the screened concentration range of PVP (3–5.2 mM) and Acacia (6.5–8.5 mM) was adopted. The synthesis parameters and average sizes of compounds **#1**, **#2**, **#3**, and **#4** are listed in Table S5. SEM images showing the morphologies and size distributions are presented in Figure S11a–h, encompassing ligand-free (500 nm), Acacia as a ligand (220 nm), PVP as a ligand (260 nm), and PVP and Acacia as ligands (310 nm). $CsPbBr_3$ crystals grown without ligands exhibit random sizes and morphologies because of their uncontrolled growth.[31] Upon the addition of Acacia, the $CsPbBr_3$ crystals exhibited a cubic morphology. PVP micelles may form when the PVP concentration surpasses the critical micelle concentration[32] (Figure S11c). The hydrophilic and hydrophobic groups of PVP enabled the rearrangement of PVP molecules in the solution, leading to the formation of micelles and size manipulation.[33] These micelles confine the formation and movement of crystals[34] and self-assemble into quasi-spherical structures.[35] Size reduction and improved uni-

formity with Acacia and PVP as ligands were revealed using 100 randomly selected crystals (Figure S11e–g). PVP reduces crystal size,[36] reaching approximately 42.71 ± 28 nm (crystals on the quasi-spherical structure), as shown in Figure S11i–j. However, the size increases to 58.70 ± 22 nm with the addition of Acacia. This further confirms the role of Acacia in weakening the effect of PVP and increasing the crystal size, as reflected in the increasing slope of the absorption spectra at 400 nm to 450 nm with Acacia concentration exceeding 9.5 mM (Figure 2d). Therefore, Acacia enhanced crystallinity, while PVP promoted the formation of quasi-spherical structures and regulated size, as verified via XRD (Figure S11k–l). Due to the formation of quasi-spherical $CsPbBr_3$ by both, the interaction between Acacia and PVP is minimal.

It should be noted that, Acacia is comprised of galactose, arabinose, rhamnose, glucuronic acid, etc.[37] Among them, glucuronic acid with a carbonyl group shows specific chemical properties.[35] Here, the glucuronic acid is supposed to be the main active ligands, and the carbonyl group may play a role in improving crystallinity. Figures 3a and b show that the addition of Acacia led to the formation of cubic crystals, whereas irregular crystals were obtained without ligands. Figures 3c and d, along with Figure S12, show that the crystal arrangement within the micelles varied. When PVP was used as a ligand, the $CsPbBr_3$ NCs within the micelles exhibited irregular arrangements. However, when both Acacia and PVP were used as ligands, $CsPbBr_3$ NCs inside the micelles exhibited regularity, aligning in a specific direction with a certain orientation. This regularity may be associated with the selective adsorption of glucuronic acid from Acacia, similar to the selective adsorption of butylamine ions, which enables the directional growth of lead-free perovskite crystals.[38] The XRD patterns of **#1** and **#2** were normalized to the (200) peak intensity. The ratios of the (100) peak intensities of **#1** and **#2** to the (100) peak intensity of the cubic phase of $CsPbBr_3$ (PDF#54-0752) were 1.506 and 1.823, respectively, whereas the ratios for the (110) facet were 0.865 and 0.648, respectively.[39] This suggests that the growth of $CsPbBr_3$ NCs along the [110] direction was inhibited and more inclined to grow along the [100] direction. Furthermore, the adsorption energy of the

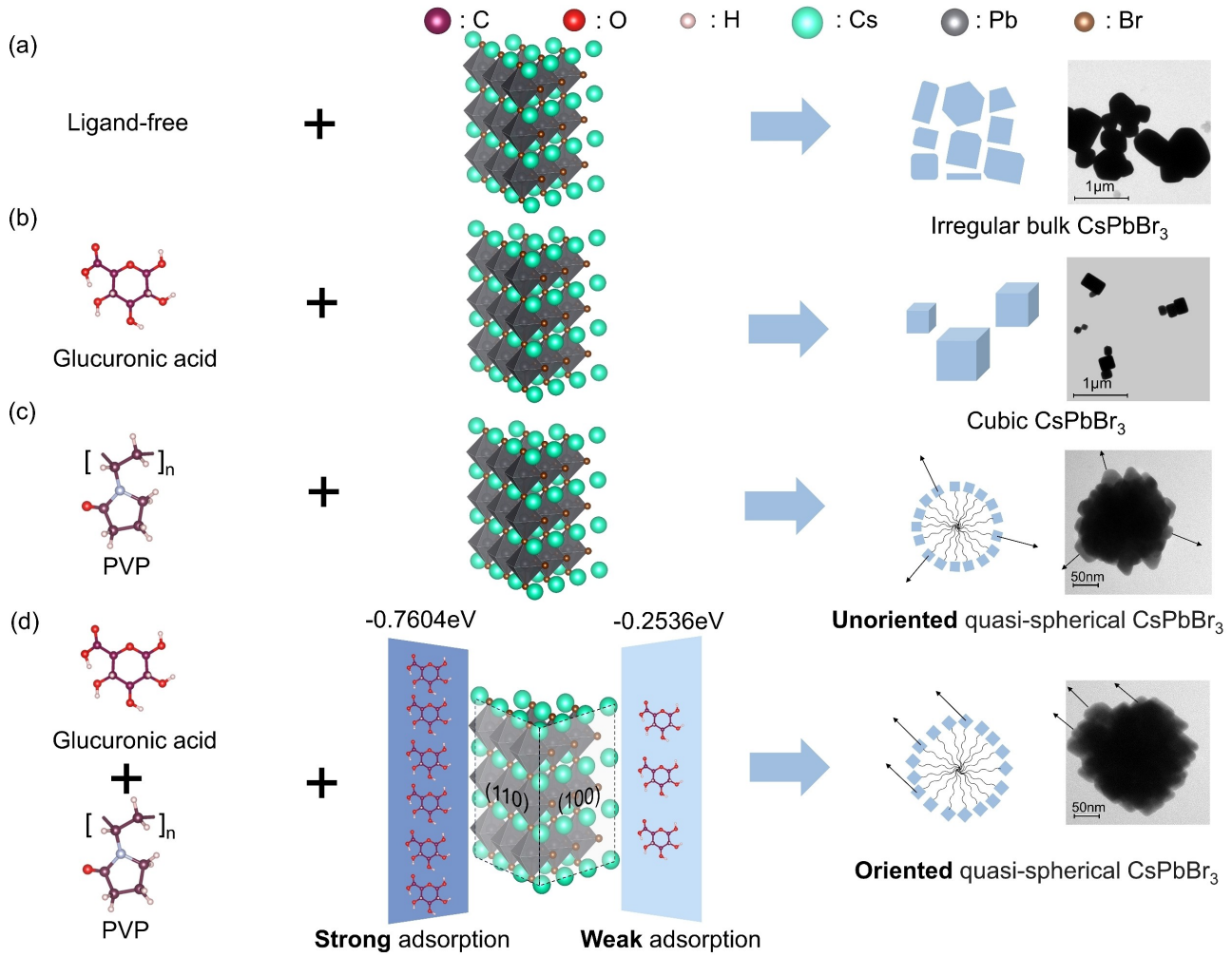

Figure 3. Mechanism of the morphology-controlled synthesis of oriented quasi-spherical $CsPbBr_3$ perovskites. TEM images showing the (a) irregular bulk morphology of $CsPbBr_3$ grown ligand-free, (b) cubic morphology of $CsPbBr_3$ with Acacia as a ligand, (c) unoriented quasi-spherical $CsPbBr_3$ with PVP as a ligand, and (d) oriented quasi-spherical $CsPbBr_3$ with Acacia and PVP as ligands.

glucuronic acid on the (100) facet was −0.2536 eV, increasing to −0.7604 eV on the (110) facet (details are provided in the Supporting Information and Figure S13). Strong adsorption inhibited crystal facet growth along the [110] direction of NCs on micelles, leading to growth along the [100] direction, thus promoting the oriented growth of NCs on micelles.

Data-driven analysis of 652 G values and 688 absorption spectra highlights the superiority of the **#4** formula within the screened concentration range. Figure S14a shows the PL lifetimes and PLQYs for **#1**, **#2**, **#3**, and **#4** formulas. The corresponding PLQYs under 365 nm excitation light were lower than 1 %, 8.29 %, 2.84 %, and 10.18 %, respectively. Under excitation conditions with a wavelength of 365 nm and emission at 526 nm, the corresponding PL lifetimes were 3.51, 32.96, 14.05, and 35.00 ns, respectively. Owing to the lattice disruption caused by polar solvents and non-radiative recombination,[31] the **#1** formula exhibited the lowest optical properties. Meanwhile, the optical properties of formula **#3** were slightly improved, possibly owing to the protection provided by the micelles. The enhancement observed between **#2** and **#4** may be attributed to both PVP-provided micelles and the improved crystallinity facilitated by acacia. Moreover, the oriented quasi-spherical $CsPbBr_3$ structure synthesized using the **#4** formula showed better stability against polar solvents and air (Figure S14b–c). Therefore, we believe that the utilization of diverse ligands may be a prospective direction for future research in perovskite synthesis.

In summary, controlled synthesis of oriented quasi-spherical $CsPbBr_3$ perovskites is likely to be achieved through data-driven strategies. The unique effects of PVP and Acacia on $CsPbBr_3$ were investigated via high-throughput characterization. Furthermore, the synthesis parameters were optimized using data-driven approaches, resulting in enhanced optical properties of $CsPbBr_3$ crystals. Furthermore, through the integration of ML, ex situ characterization, and DFT calculations, the mechanism for morphology-controlled synthesis was elucidated, potentially enabling the controlled arrangement of crystals on quasi-spherical

$CsPbBr_3$ perovskite. The investigation into how adsorption energy influences $CsPbBr_3$ crystal growth direction is consistent with the reported perovskite single-crystal facet control.[40] We anticipate that data-driven controlled synthesis will provide more possibilities for the design and synthesis of perovskite materials and accelerate the identification of correlations between big data and high-throughput experiments to achieve more precise perovskite synthesis. Data-driven strategies are expected to expedite the controlled synthesis of various crystal materials, enabling the directed synthesis of materials with specific properties.

Supporting Information

The authors have cited additional references within the Supporting Information.

Acknowledgements

This work was supported by the National Natural Science Foundation of China (52173234), Shenzhen Science and Technology Program Grant No. RCJC20200714114435061, Shenzhen Science and Technology Program (JCY20210324102008023 and JSGG20210802153408024), Shenzhen-Hong Kong-Macau Technology Research Program (Type C, SGDX2020110309300301), Natural Science Foundation of Guangdong Province (2022A1515010554 and 2022A1515011959), Open Project of ZhengZhou JiShu Institute of AI Science (ZZJSB2023001). J. Y. and R. L. Z. H. were supported by the UK Research and Innovation through a Frontier Grant (no. EP/X022900/1), awarded through the 2021 ERC Starting Grant scheme. R. L. Z. H. also thanks the Royal Academy of Engineering for support through the Research Fellowships programme (no. RF \201718\17101). We thank Prof. Guohua Zhong (Centre for Photonics Information and Energy Materials, Shenzhen Institute of Advanced Technology, Chinese Academy of Sciences, PR China) for his help to this work. Shenzhen Science and Technology Program (ZDSYS20220606100606013).

Conflict of Interest

The authors declare no conflict of interest.

Data Availability Statement

The data that support the findings of this study are available from the corresponding author upon reasonable request.

Keywords: Data-driven · Controlled synthesis · Perovskite

[1] a) C. Otero-Martínez, J. Ye, J. Sung, I. Pastoriza-Santos, J. Pérez-Juste, Z. Xia, A. Rao, R. L. Hoye, L. Polavarapu, *Adv. Mater.* **2022**, *34*, 2107105; b) G. Wang, Y. Sun, D. Li, H. W. Liang, R. Dong, X. Feng, K. Müllen, *Angew. Chem. Int. Ed.* **2015**, *127*, 15406–15411.

[2] a) L. Zhou, Z. Zhuang, H. Zhao, M. Lin, D. Zhao, L. Mai, *Adv. Mater.* **2017**, *29*, 1602914; b) S. Chen, H. Su, Y. Wang, W. Wu, J. Zeng, *Angew. Chem. Int. Ed.* **2015**, *127*, 110–115.

[3] a) P. K. Baviskar, P. R. Nikam, S. S. Gargote, A. Ennaoui, B. R. Sankapal, *J. Alloys Compd.* **2013**, *551*, 233–242; b) K. Chen, H. Tüysüz, *Angew. Chem. Int. Ed.* **2015**, *54*, 13806–13810.

[4] T. Güner, G. Topçu, U. Savacı, A. Genç, S. Turan, E. Sari, M. M. Demir, *Nanotechnology* **2018**, *29*, 135202.

[5] L. Lv, Y. Xu, H. Fang, W. Luo, F. Xu, L. Liu, B. Wang, X. Zhang, D. Yang, W. Hu, *Nanoscale* **2016**, *8*, 13589–13596.

[6] X. Du, G. Wu, J. Cheng, H. Dang, K. Ma, Y.-W. Zhang, P.-F. Tan, S. Chen, *RSC Adv.* **2017**, *7*, 10391–10396.

[7] a) Q. Zhou, S. Lu, Y. Wu, J. Wang, *J. Phys. Chem. Lett.* **2020**, *11*, 3920–3927; b) F. Lai, Z. Sun, S. E. Saji, Y. He, X. Yu, H. Zhao, H. Guo, Z. Yin, *Small* **2021**, *17*, 2100024; c) L. Xing, Z. Chen, W. Chen, P. K. Chu, X.-F. Yu, H. Zhao, *Chem. Eng. J.* **2023**, *466*, 143225; d) H. Li, Y. Jiao, K. Davey, S. Z. Qiao, *Angew. Chem. Int. Ed.* **2023**, *135*, e202216383; e) C. t. Yang, Y. Wang, E.

Marutani, T. Ida, X. Ni, S. Xu, W. Chen, H. Zhang, T. Akaike, F. Ichinose, *Angew. Chem. Int. Ed.* **2019**, *58*, 10898–10902.
[8] a) Z. Wang, Z. Sun, H. Yin, X. Liu, J. Wang, H. Zhao, C. H. Pang, T. Wu, S. Li, Z. Yin, *Adv. Mater.* **2022**, *34*, 2104113; b) L. Himanen, A. Geurts, A. S. Foster, P. Rinke, *Adv. Sci.* **2019**, *6*, 1900808; c) D. H. Mok, H. Li, G. Zhang, C. Lee, K. Jiang, S. Back, *Nat. Commun.* **2023**, *14*, 7303.
[9] a) C. Draxl, M. Scheffler, *MRS Bull.* **2018**, *43*, 676–682; b) H. Zhao, W. Chen, H. Huang, Z. Sun, Z. Chen, L. Wu, B. Zhang, F. Lai, Z. Wang, M. L. Adam, *Nat. Synth.* **2023**, 505–514.
[10] J. N. Cawse, *Acc. Chem. Res.* **2001**, *34*, 213–221.
[11] M. Li, D. Liu, D. Wei, X. Song, D. Wei, A. T. S. Wee, *Adv. Sci.* **2016**, *3*, 1600003.
[12] Q. Fan, G. V. Biesold-McGee, J. Ma, Q. Xu, S. Pan, J. Peng, Z. Lin, *Angew. Chem. Int. Ed.* **2020**, *59*, 1030–1046.
[13] B. Zhou, D. Yan, *Angew. Chem. Int. Ed.* **2019**, *131*, 15272–15279.
[14] M. R. Filip, G. E. Eperon, H. J. Snaith, F. Giustino, *Nat. Commun.* **2014**, *5*, 5757.
[15] J. H. Joo, R. Merkle, J. Maier, *J. Power Sources* **2011**, *196*, 7495–7499.
[16] D. Wang, W. Li, Z. Du, G. Li, W. Sun, J. Wu, Z. Lan, *J. Mater. Chem. C* **2020**, *8*, 1649–1655.
[17] Q. Zhong, M. Cao, Y. Xu, P. Li, Y. Zhang, H. Hu, D. Yang, Y. Xu, L. Wang, Y. Li, *Nano Lett.* **2019**, *19*, 4151–4157.
[18] H. Zhu, Y. Pan, C. Peng, H. Lian, J. Lin, *Angew. Chem. Int. Ed.* **2022**, *61*, e202116702.
[19] a) B. Wang, J. Peng, X. Yang, W. Cai, H. Xiao, S. Zhao, Q. Lin, Z. Zang, *Laser Photonics Rev.* **2022**, *16*, 2100736; b) W. Yin, M. Li, W. Dong, X. Zhang, W. Zheng, *Angew. Chem. Int. Ed.* **2023**, e202303462.
[20] a) L. Song, X. Guo, Y. Hu, Y. Lv, J. Lin, Z. Liu, Y. Fan, X. Liu, *J. Phys. Chem. Lett.* **2017**, *8*, 4148–4154; b) Y. Zhang, S. Chen, H. Chen, G. Zhang, M. Zhao, C. Zhao, W. Guo, W. Ji, Z. Shi, T. Jiu, *J. Mater. Chem. C* **2020**, *8*, 5894–5903; c) J. Zhu, B. He, Z. Gong, Y. Ding, W. Zhang, X. Li, Z. Zong, H. Chen, Q. Tang, *ChemSusChem* **2020**, *13*, 1834–1843; d) Y. Xu, W. Zhang, K. Su, Y. X. Feng, Y. F. Mu, M. Zhang, T. B. Lu, *Chem. Eur. J.* **2021**, *27*, 2305–2309; e) X. Wang, D. Liu, R. Liu, X. Du, B. Zhang, X. Sun, C. Chen, Z. Li, Q. Zhao, Z. Shao, *Adv. Energy Mater.* **2023**, *13*, 2203635.
[21] a) H. Jiang, Z. Yan, H. Zhao, S. Yuan, Z. Yang, J. Li, B. Liu, T. Niu, J. Feng, Q. Wang, *ACS Appl. Energ. Mater.* **2018**, *1*, 900–909; b) H. Zhang, M. K. Nazeeruddin, W. C. Choy, *Adv. Mater.* **2019**, *31*, 1805702; c) L. Zhu, X. Zhang, M. Li, X. Shang, K. Lei, B. Zhang, C. Chen, S. Zheng, H. Song, J. Chen, *Adv. Energy Mater.* **2021**, *11*, 2100529.
[22] a) N. S. Pesika, K. J. Stebe, P. C. Searson, *J. Phys. Chem. B* **2003**, *107*, 10412–10415; b) J. Thessing, J. Qian, H. Chen, N. Pradhan, X. Peng, *J. Am. Chem. Soc.* **2007**, *129*, 2736–2737; c) D. L. Ferreira, J. Sousa, R. Maronesi, J. Bettini, M. Schiavon, A. V. Teixeira, A. G. Silva, *J. Chem. Phys.* **2017**, *147*.
[23] a) B.-E. Cohen, T. Binyamin, T. Ben-Tzvi, O. Goldberg, A. Schlesinger, I. Balberg, O. Millo, E. Gross, D. Azulay, L. Etgar, *ACS Energy Lett.* **2021**, *7*, 217–225; b) H. Kim, J. Hong, C. Kim, E.-Y. Shin, M. Lee, Y.-Y. Noh, B. Park, I. Hwang, *J. Chem. Phys.* **2018**, *122*, 16630–16638.
[24] a) Y.-R. Shi, K.-L. Wang, Y.-H. Lou, D.-B. Zhang, C.-H. Chen, J. Chen, Y.-X. Ni, S. Öz, Z.-K. Wang, L.-S. Liao, *Nano Energy* **2022**, *97*, 107200; b) J. Ye, M. M. Byranvand, C. O. Martínez, R. L. Hoye, M. Saliba, L. Polavarapu, *Angew. Chem. Int. Ed.* **2021**, *133*, 21804–21828; c) N. Fiuza-Maneiro, K. Sun, I. López-Fernández, S. Gómez-Graña, P. Müller-Buschbaum, L. Polavarapu, *ACS Energy Lett.* **2023**, *8*, 1152–1191.
[25] C. Shen, Y. Zhao, L. Yuan, L. Ding, Y. Chen, H. Yang, S. Liu, J. Nie, W. Xiang, X. Liang, *Chem. Eng. J.* **2020**, *382*, 122868.
[26] Q. A. Akkerman, T. P. Nguyen, S. C. Boehme, F. Montanarella, D. N. Dirin, P. Wechsler, F. Beiglböck, G. Rainò, R. Erni, C. Katan, *Science* **2022**, *377*, 1406–1412.
[27] a) L. Guo, Y. Gu, Z. Yang, S. Tian, X. San, J. Liu, L. Gao, S. Qiao, S. Wang, *Adv. Mater. Interfaces* **2021**, *8*, 2002231; b) Y. Li, R. Lai, X. Luo, X. Liu, T. Ding, X. Lu, K. Wu, *Chem. Sci.* **2019**, *10*, 5983–5989; c) K. Wei, X. Zheng, X. Cheng, C. Shen, T. Jiang, *Adv. Opt. Mater.* **2016**, *4*, 1993–1997.
[28] a) J. Maes, L. Balcaen, E. Drijvers, Q. Zhao, J. De Roo, A. Vantomme, F. Vanhaecke, P. Geiregat, Z. Hens, *J. Phys. Chem. Lett.* **2018**, *9*, 3093–3097; b) P. Cottingham, R. L. Brutchey, *Chem. Commun.* **2016**, *52*, 5246–5249; c) Y. Xian, Y. Zhang, N. U. Rahman, H. Yin, Y. Long, P. Liu, W. Li, J. Fan, *J. Phys. Chem. C* **2020**, *124*, 13434–13446; d) P. Zhang, Y. Hua, X. Li, L. Zhang, L. Liu, R. Li, G. Zhang, X. Tao, *J. Mater. Chem. C* **2021**, *9*, 2840–2847; e) J. Chen, K. Zidek, P. Chábera, D. Liu, P. Cheng, L. Nuuttila, M. J. Al-Marri, H. Lehtivuori, M. E. Messing, K. Han, *J. Phys. Chem. Lett.* **2017**, *8*, 2316–2321; f) M. C. Brennan, J. E. Herr, T. S. Nguyen-Beck, J. Zinna, S. Draguta, S. Rouvimov, J. Parkhill, M. Kuno, *J. Am. Chem. Soc.* **2017**, *139*, 12201–12208; g) J. Chen, P. Chábera, T. Pascher, M. E. Messing, R. Schaller, S. Canton, K. Zheng, T. Pullerits, *J. Phys. Chem. Lett.* **2017**, *8*, 5119–5124; h) Y. Li, T. Ding, X. Luo, Z. Chen, X. Liu, X. Lu, K. Wu, *Nano Res.* **2019**, *12*, 619–623; i) N. Tabassum, Z. N. Georgieva, G. H. Debnath, D. H. Waldeck, *Nanoscale* **2023**, *15*, 2143–2151; j) F. Krieg, P. C. Sercel, M. Burian, H. Andrusiv, M. I. Bodnarchuk, T. Stöferle, R. F. Mahrt, D. Naumenko, H. Amenitsch, G. Rainò, *ACS Cent. Sci.* **2020**, *7*, 135–144.
[29] S. H. Chang, W.-C. Huang, C.-C. Chen, S.-H. Chen, C.-G. Wu, *Appl. Surf. Sci.* **2018**, *445*, 24–29.
[30] a) R. Ouyang, E. Ahmetcik, C. Carbogno, M. Scheffler, L. M. Ghiringhelli, *J. Phys. Condens. Matter* **2019**, *2*, 024002; b) R. Ouyang, S. Curtarolo, E. Ahmetcik, M. Scheffler, L. M. Ghiringhelli, *Phys. Rev. Mater.* **2018**, *2*, 083802.
[31] Y. Sun, H. Zhang, K. Zhu, W. Ye, L. She, X. Gao, W. Ji, Q. Zeng, *RSC Adv.* **2021**, *11*, 27333–27337.
[32] a) D. N. Rubingh, in *Solution Chemistry of Surfactants: Volume 1*, Springer, **1979**, pp. 337–354; b) K. Prochazka, T. J. Martin, S. E. Webber, P. Munk, *Macromolecules* **1996**, *29*, 6526–6530; c) K. Chari, *J. Colloid Interface Sci.* **1992**, *151*, 294–296.
[33] a) C. Tanford, *J. Mol. Biol.* **1972**, *67*, 59–74; b) K. D. K. Kenkyūjo, *Bull. inst. chem. res., Kyoto univ.*, Institute for Chemical Research, Kyoto University., **1958**; c) N. Wang, X. Wang, L. Yang, H. Chen, *Micro Nano Lett.* **2013**, *8*, 94–98; d) J. Chandradass, K. H. Kim, *J. Cryst.* **2009**, *311*, 3631–3635.
[34] F. M. Menger, *Acc. Chem. Res.* **1979**, *12*, 111–117.
[35] A. Nakajima, H. Sato, *Bull. Inst. Chem. Res. Kyoto Univ.* **1968**, *47*, 177–183.
[36] K. M. Koczkur, S. Mourdikoudis, L. Polavarapu, S. E. Skrabalak, *Dalton Trans.* **2015**, *44*, 17883–17905.
[37] C. Sanchez, M. Nigen, V. M. Tamayo, T. Doco, P. Williams, C. Amine, D. Renard, *Food Hydrocolloids* **2018**, *78*, 140–160.
[38] a) B. Li, Y. Zhang, L. Fu, T. Yu, S. Zhou, L. Zhang, L. Yin, *Nat. Commun.* **2018**, *9*, 1076; b) W. Wang, M. Cai, G. Wu, L. Zhu, X. Liu, H. Lv, S. Dai, *Cryst. Growth Des.* **2021**, *21*, 5840–5847.
[39] G. Murugadoss, G. Mizuta, S. Tanaka, H. Nishino, T. Umeyama, H. Imahori, S. Ito, *APL Mater.* **2014**, *2*.
[40] Y. Jin, Z. K. Wang, S. Yuan, Q. Wang, C. Qin, K. L. Wang, C. Dong, M. Li, Y. Liu, L. S. Liao, *Adv. Funct. Mater.* **2020**, *30*, 1908339.

Manuscript received: December 17, 2023
Accepted manuscript online: February 5, 2024
Version of record online: February 29, 2024